Membrane lipidome of an epithelial cell line

Julio L. Sampaio[a,1,2], Mathias J. Gerl[a,1], Christian Klose[a], Christer S. Ejsing[b], Hartmut Beug[c], Kai Simons[a,2], and Andrej Shevchenko[a,2]

[a]Max Planck Institute of Molecular Cell Biology and Genetics, 01307 Dresden, Germany; [b]Department of Biochemistry and Molecular Biology, University of Southern Denmark, 55 Campusvej, DK-5230 Odense, Denmark; and [c]Research Institute of Molecular Pathology, 1030 Vienna, Austria

Contributed by Kai Simons, December 22, 2010 (sent for review December 7, 2010)

Tissue differentiation is an important process that involves major cellular membrane remodeling. We used Madin–Darby canine kidney cells as a model for epithelium formation and investigated the remodeling of the total cell membrane lipidome during the transition from a nonpolarized morphology to an epithelial morphology and vice versa. To achieve this, we developed a shotgun-based lipidomics workflow that enabled the absolute quantification of mammalian membrane lipidomes with minimal sample processing from low sample amounts. Epithelial morphogenesis was accompanied by a major shift from sphingomyelin to glycosphingolipid, together with an increase in plasmalogen, phosphatidylethanolamine, and cholesterol content, whereas the opposite changes took place during an epithelial-to-mesenchymal transition. Moreover, during polarization, the sphingolipids became longer, more saturated, and more hydroxylated as required to generate an apical membrane domain that serves as a protective barrier for the epithelial sheet.

epithelial polarity | shotgun lipidomics | high resolution mass spectrometry | Forssman glycosphingolipid | epithelial-mesenchymal transition

Gain and loss of epithelial polarity are fundamental processes in tissue differentiation (1, 2). These processes have been extensively studied not only in the context of embryogenesis but in tumor progression and metastasis (1). Although cell polarization necessarily implies major changes in the structure and properties of the cell membranes, the exact changes in the molecular composition of their membrane lipidome remain unknown.

Madin–Darby canine kidney (MDCK) cells are a cell culture model for epithelial polarization (3, 4). When seeded at low density, MDCK cells undergo a morphological change from a fibroblast-like morphology to a well-polarized epithelium (5) and have recently also been adapted to undergo an epithelial-mesenchymal transition (EMT) (6). Epithelial cells have evolved characteristic apical and basolateral membrane domains, separated by tight junctions, with specific protein and lipid composition (7, 8). The unusual robustness of the apical membrane is largely attributable to its special lipid composition (9–11).

In this work, we applied shotgun MS for comprehensive and quantitative characterization of mammalian cellular membranes (12). By combining high mass resolution MS, an improved extraction procedure that increases the recovery of polar lipids (13), and the use of internal standard mixtures for absolute quantification, we expanded the lipid repertoire covered by shotgun lipidomics to glycosphingolipids (GSPs). Importantly, the analysis of the GSPs did not require the hydrolysis of glycerophospholipids (GPs) (14), and this simplification allowed us to determine the membrane lipidome with unprecedented comprehensiveness (more than 300 lipid species from 14 different lipid classes) from a single sample of 10^5 cells.

We further elucidated how the lipidome is remodeled during the course of MDCK cell epithelial polarization. We found that when these cells change from a fibroblastoid to a polarized epithelial phenotype, there was a profound remodeling of their lipidome. Sphingolipids (SPs), with the progression of polarization, became longer, more saturated, more hydroxylated, and more glycosylated. Conversely, the GPs generally acquired longer and more unsaturated fatty acids. Moreover, these changes seem to be specific to the cell state because we could recapitulate the changes in the lipidome when MDCK cells depolarized toward a mesenchymal state.

Results

Shotgun Quantification of Mammalian GSPs. Shotgun lipidomics have allowed absolute quantification of GPs by MS-based methods and provided a reliable workflow for comprehensive quantitative characterization of GPs,* some SPs, and sterols (15–17). A recently developed extraction procedure has enabled the expansion of the lipid repertoire to highly polar lipids that were not efficiently recovered by conventional methods (13). We extracted the same amount of harvested MDCK cells by a modification of this two-step protocol (13) and by Folch extraction (18) and compared them by TLC (Fig. S1). We observed that in the two-step extraction, the GSP recovery was markedly increased. MS analysis of the extracts showed a 10-fold gain in intensity of GSP peaks in comparison with the Folch extract. We identified the specific complex GSP classes of epithelial MDCK cells (19): the ganglioside GM3, galactosylceramide-sulfate (Sulf), and the globoside derivative Forssman glycolipid (For).

In shotgun lipidomics, absolute quantification of lipid species relies on a single synthetic lipid standard comprising nonendogenous fatty acid moieties. At least one such standard per each analyzed lipid class is spiked into the cell lysate before the extraction (16). Because no synthetic standards are available for GM3 and For, we developed a quantification method that used standards purified from natural sources. The species composition of the standard differed from the composition of MDCK cells (Fig. S2 *A* and *B*); thus, it was possible to quantify the endogenous species using the intensities of nonoverlapping species (Fig. S2 *A* and *B* and *SI Materials and Methods*). The quantification dynamic range for GM3 and For was better than two orders of magnitude, with a limit of quantification of 1 pmol (Fig. S2 *C* and *D*).

Lipidome Changes During an EMT. To investigate the total cell lipidome changes in an EMT, we used an engineered MDCK cell line stably expressing an estrogen-inducible and constitutively active Raf1 mutant protein (MDCK-DDRafER) (20) and developed an assay to allow EMT induction even in dense cultures that would promote full epithelial polarization in control cells. In contrast to the control epithelial cells, the treated cells showed a mesenchymal morphology and were lacking the epithelial markers E-cadherin

Author contributions: J.L.S., M.J.G., and K.S. designed research; J.L.S., M.J.G., C.K., and H.B. performed research; J.L.S., C.S.E., H.B., and A.S. contributed new reagents/analytic tools; J.L.S. and C.K. analyzed data; and J.L.S., M.J.G., K.S., and A.S. wrote the paper.

The authors declare no conflict of interest.

[1]J.L.S. and M.J.G. contributed equally to this work.

[2]To whom correspondence may be addressed. E-mail: sampaio@mpi-cbg.de, simons@mpi-cbg.de, or shevchenko@mpi-cbg.de.

This article contains supporting information online at www.pnas.org/lookup/suppl/doi:10.1073/pnas.1019267108/-/DCSupplemental.

*For simplicity, we include the glycerolipid DAG in the GP category.

CELL BIOLOGY

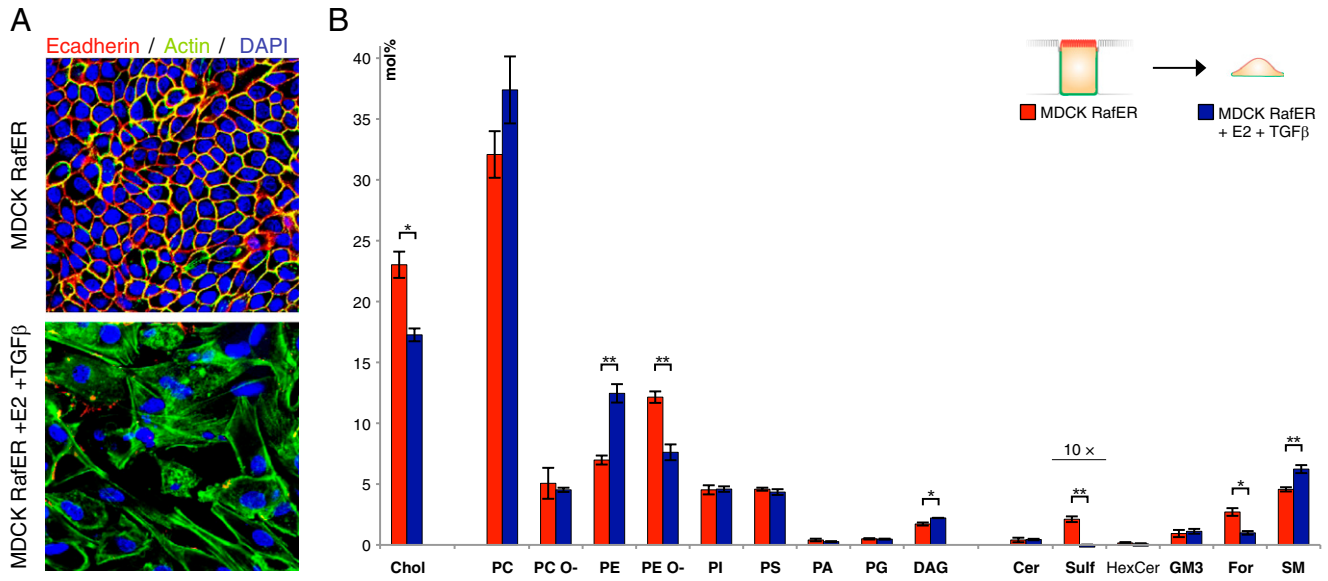

Fig. 1. Lipidomics of an EMT. (*A*) (*Lower*) EMT was introduced in MDCK B cells transformed with an estrogen-inducible and constitutively active Raf1 mutant and cultured in the presence of estrogen and TGF-β. (*Upper*) Uninduced cells serve as a control. After 4 d, cells were stained for E-cadherin, actin, and nuclei (DAPI). (*B*) Lipid class compositions of cells that have undergone an EMT compared with control cells. The content of individual lipid classes was determined by summing up absolute abundances of all identified species and is expressed as mol%. An unpaired *t* test with Welch's correction was used to estimate the *P* values: $*P < 0.05$; $**P < 0.01$. Error bars correspond to SD ($n = 3$).

and ZO-1 but were now expressing the mesenchymal markers vimentin and fibronectin (Fig. 1*A* and Fig. S3).

We observed profound changes in the lipidome during the EMT (Fig. 1*B*, Dataset S1). Notably, the increase of sphingomyelin (SM) content was compensated for by a decrease in For and Sulf when cells became mesenchymal. Moreover, we observed an increase in diacylglycerol (DAG) and an apparent conversion of plasmalogen (PE O-) to diacyl-phosphatidylethanolamine (PE) in the mesenchymal state. Cholesterol (Chol) content in the unpolarized cells was markedly decreased. At the lipid species level, we observed lesser yet significant changes (Fig. S4).

Changes in Lipidome During the Polarization of MDCK Cells. The previous experiments suggest a highly specific regulation of the MDCK cellular lipidome, which correlated with the polarization state. To characterize the "dynamics" of these lipidomic changes and their reversibility, we investigated the time-resolved total cell lipidome during the formation of an epithelial monolayer with apical and basolateral surface domains over a time course of 13 d (Fig. 2*A*). Initially, cells were sparsely distributed, spread out, and flat, but they grew denser on day 3, forming cell-cell contacts and separate apical and basolateral domains. This differentiation process resulted in an epithelial monolayer from day 5 onward. Annexin 13, which has been implicated in raft-mediated apical transport (21) and is absent in the early stages of epithelium formation in Caco-2 cells (22), was only visible after the epithelium had formed (Fig. 2*B*).

During progression to the epithelial state, the GP class profile did not change with the exception of a conversion of PE to PE O- and a slight decrease of DAGs (Fig. 3*A*, Fig. S5*A* and Dataset S1). SM and GM3 were the most abundant SP classes at the onset of polarization (days 1 and 3). With the establishment of the epithelium (starting from days 5–13), we observed a drastic increase of Sulf and For (with the latter not being detectable from days 1–3). Remarkably, Chol dropped on days 3–5, although increasing again with the progression of epithelial formation (days 5–13) (as observed for the EMT), suggesting that these time points (3–5 d) should mark the end of the cell proliferation phase and the beginning of cell polarization. All the observed differences confirmed that the lipidomic remodeling observed during the EMT indeed correlated with the polarization status. This was also confirmed by principal component analysis (PCA), which separates the polarized state from the unpolarized state during the EMT in the same way as during the polarization time course (Fig. S5*D*).

Unpolarized MDCK cells (days 3–5) were relatively enriched in GP species with shorter [carbon atoms (C) = 34 and 36] and more saturated [double bonds (db) = 1 and 2] (Fig. 3 *B* and *C*) fatty acids than the epithelial states (days 7–13). These changes were compensated for by the enrichment in longer ($C > 36$) and more unsaturated ($db > 3$) fatty acid moieties (Fig. 3 *B* and *C*) in the epithelial states. For SPs, we also observed a strong depletion of shorter ($C = 34$) and more unsaturated ($db \geq 1$) SPs and a significant enrichment of all the longer ($C > 36$) and fully saturated lipid species during the epithelial progression of MDCK cells (Fig. 3 *D* and *E*). We also observed an increase of SP species with three hydroxylations and depletion of SP species with two hydroxylations during the progression in cell polarization (Fig. 3*F*). This was not reflected in all SP classes, however. Although additional hydroxylations were almost absent in SM, they were strongly increased in For and GM3 but were surprisingly depleted in Sulf (Fig. 3*G*).

Discussion

Although the current lipidomic methodologies have succeeded in elucidating the molecular composition of major GP classes, complex GSPs were neglected within common lipidomic routines (14, 23–25). These lipid classes, however, are both biologically important and abundant (19, 26, 27). To amend this deficiency, we first optimized the two-stage lipid extraction. Using a combination of TLC and shotgun MS, we demonstrated enhanced recovery of the major mammalian GSPs and their detection at the low picomole level within a dynamic range better than 100×. Importantly, GSP profiling remains fully integrated into the shotgun lipidomics pipeline. High mass resolution of an LTQ-Orbitrap instrument enabled unequivocal assignment of species via their m/z , which was determined with a sub-ppm mass accuracy, hence eliminating the need of MS/MS (28, 29).

Therefore, it has become possible to profile the lipidome of GSP-rich MDCK cells (19) and to track the lipidomic changes during epithelial polarization at the level of individual molecular species.

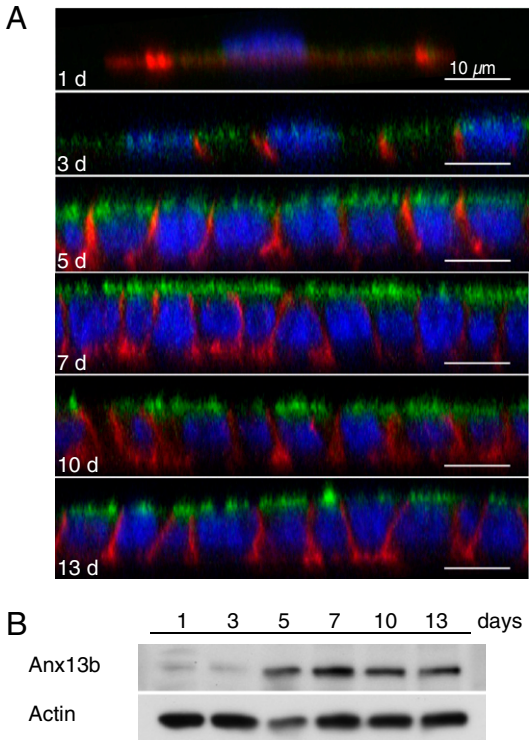

Fig. 2. Time course of polarization. MDCK cells were rendered contact-naive by culturing at low density for 3 d, seeded at low density on filters, and allowed to grow for the indicated time periods. (*A*) Cells were immunostained for podocalyxin (green), β-catenin (red), and nuclei (blue, DAPI). The *x-z* views of confocal stacks are shown. (*B*) Immunoblotting analysis of the respective samples for annexin 13b. Equal loading was confirmed by reprobing for β-actin.

We observed pronounced changes in the abundance of DAG as well as in the remodeling of PE and SP composition. Particularly striking was the change from an SM-dominated subconfluent cell to a GSP-rich epithelial cell. DAG is produced from the synthesis of SM; thus, it is expected that the DAG content correlates with the levels of SM (30). Because of the abrupt decrease in SM and the slow increase of the complex GSP For, the total SP content was reduced at the early epithelial time points (days 3–7). The drop in SPs leads to a similar decrease in Chol and an increase in GPs at the same time points (Fig. 3*A*, *Inset*). This link between Chol and SP levels could be a direct result of their physical association. Reducing SP levels would therefore increase the amount of free Chol that negatively feeds back on sterol metabolism (31). Strikingly, all these changes in the lipidome that characterized the polarization of MDCK cells became reversed during the EMT.

The changes in SP composition also extend to their lipid species. These were characterized by an increase in fatty acid chain length, hydroxylation, and saturation of SPs. To interpret the changes in the lipidomes, we have to consider the most important morphological transformation in cell membrane architecture: the introduction of an apical membrane in the polarized epithelial state. The raft concept was originally put forward to explain the biogenesis of this specialized plasma membrane domain (9), and we previously demonstrated that the apical membrane in MDCK cells is behaving as a continuous (percolating) raft phase at 25 °C (32). The changes in the lipid species accompanying the polarizing MDCK cell to a polarized state conform to the creation of a robust and impermeable raft barrier. Complex GSPs like For can, together with Chol, generate a hydrogen-bonded network in the outer leaflet of the apical membrane that helps to protect the membrane against the harsh conditions of the external environment (9).

Increased SP hydroxylation enhancing this hydrogen bonding was shown to correlate with the harshness of the membrane's external environment (33). Recent in vivo data from *Drosophila* suggest that SPs also get more hydroxylated in response to sterol depletion to maintain the physical properties of their membranes (34). Along the same lines, increased saturation of the hydrocarbon chains would increase interaction with Chol (35) and longer fatty acids could promote interleaflet coupling of a raft assembly (36). Consistent with earlier raft preparations, we find increased levels of PE O- (23, 37, 38). However, only isolating the apical membrane from polarized MDCK cells will tell us whether the lipids that characterize the polarized cells are indeed enriched there, however.

Recent studies have demonstrated that the complex GSP For in MDCK cells also functions as a receptor for the lectin galectin-9 in the apical membrane (39). This lectin is secreted apically, where it binds to For and gets endocytosed. After reaching the *trans*-Golgi network, it recycles back to the apical membrane. This lectin-GSP circuit may be instrumental in maintaining apical transport in MDCK cells. As Guan et al. (40) showed in other epithelial cells, different GSPs play a role in maintaining the epithelial state, and this might be attributed to similar lectin-GSP circuits.

Furthermore, we find a gradual remodeling of lipid species profiles during epithelial polarization (Figs. S6–S8). This is exemplified in the hydroxylation of SPs, which increases in bulk, although differentially regulated on the level of the SP classes (Fig. 3 *F* and *G*). On the level of the individual species, we can partially explain the species profile of SM by the specificity of the CERT protein (41), but how other specific species end up in their lipid classes is enigmatic, let alone by the dynamic regulation shown in this study. Further research is necessary to unveil how cells dynamically tune their lipid species during developmental processes.

Taken together, by including GSPs into the shotgun lipidomics pipeline, we demonstrate that it is possible to elucidate major compositional changes in the lipidome of mammalian cells with full molecular details. These newly developed technical capabilities revealed that the MDCK lipidome changes to produce a highly protective apical membrane barrier in the polarized cell state.

Materials and Methods

Lipid Analysis. For shotgun lipidomics analysis, samples were spiked with 10 μL of internal standard lipid mixture (*SI Materials and Methods*). Ten micrograms of protein from each sample was subjected to lipid extraction executed at 4 °C, as modified from the technique of Ejsing et al. (13). Briefly, the sample was dissolved in 200 μL of 155 mM ammonium bicarbonate and then extracted with 1 mL of chloroform-methanol (10:1) for 2 h. The lower organic phase was collected, and the aqueous phase was reextracted with 1 mL of chloroform-methanol (2:1) for 1 h. The lower organic phase was collected and evaporated in vacuum desiccators at 4 °C. Lipid extracts were dissolved in 100 μL of chloroform-methanol [1:2 (vol/vol)] and subjected to quantitative lipid analysis on both a hybrid QSTAR Pulsar *i* quadrupole time-of-flight mass spectrometer (MDS Sciex) and an LTQ-Orbitrap instrument (Thermo Fisher Scientific). Samples were infused with a TriVersa NanoMate robotic nanoflow ion source (Advion Biosciences, Inc.) as described elsewhere (13). DAG, phosphatidic acid, phosphatidylserine, PE, phosphatidylinositol, and phosphatidylglycerol species were quantified by negative ion mode multiple precursor ion scanning analysis (16); phosphatidylcholine and SM species were quantified by precursor ion scanning *m/z* 184.1 in positive ion mode. Fourier transform (FT) MS analysis on an LTQ-Orbitrap instrument quantified ceramide, hexosylceramide, dihexosylceramide, and For species in positive ion mode and GM3 species in negative ion mode. Chol was quantified as described elsewhere (15).

Software. MarkerView software (MDS Sciex) was used for PCA, and digital images were prepared and analyzed using Fiji software (freely downloadable from http://pacific.mpi-cbg.de/) as well as Photoshop and Illustrator (Adobe Systems). Automated processing of acquired mass spectra and identification and quantification of detected molecular lipid species were performed with Lipid Profiler software (MDS Sciex) (16) and LipidXplorer software, which was developed in-house.

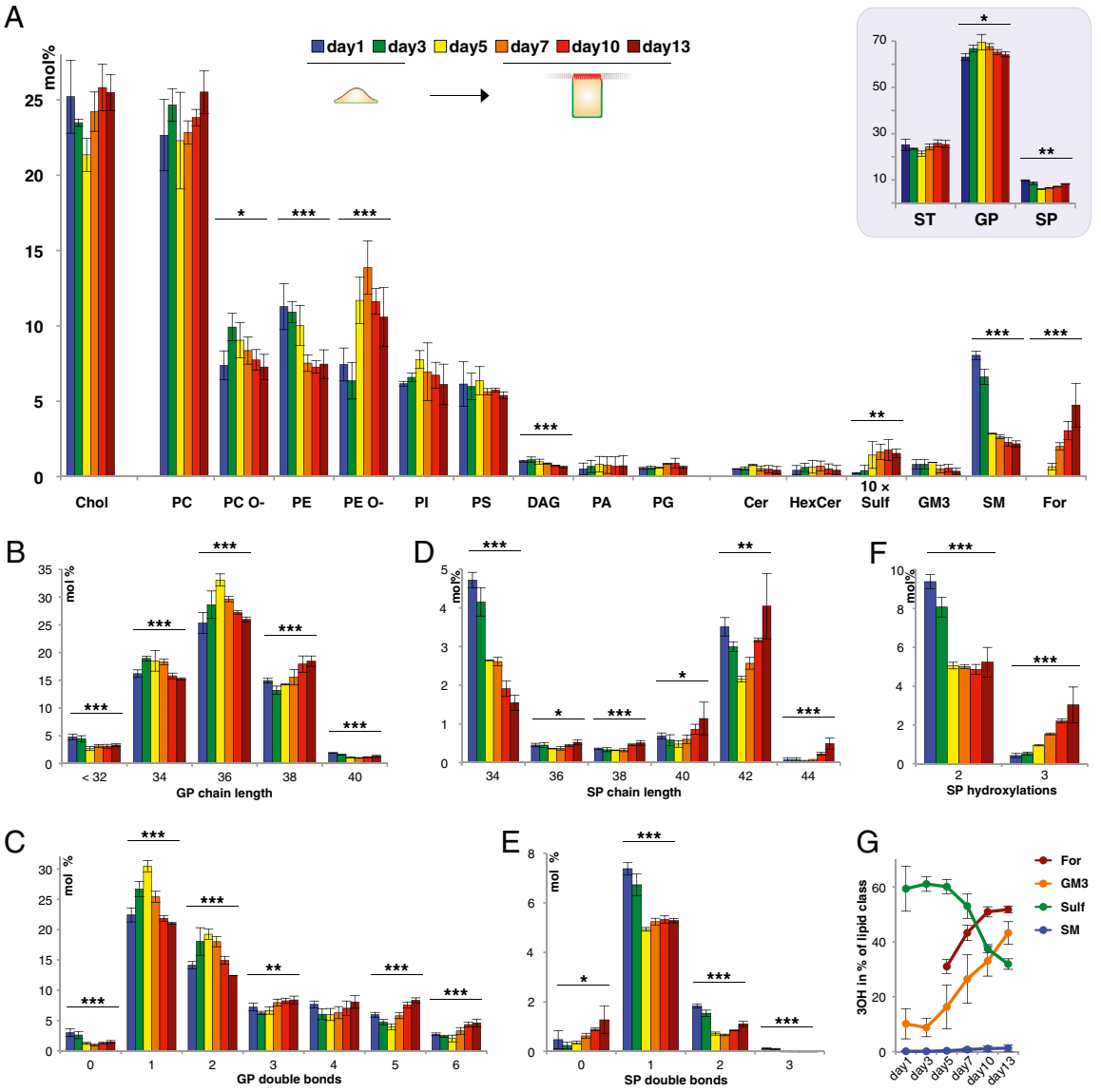

Fig. 3. Lipidomics of polarizing MDCK cells. (*A*) Lipid class compositions of polarizing MDCK cells; the content of individual lipid classes was determined as described in Fig. 1. (*Inset*) Cumulative changes within all GPs, SPs, and sterol lipids (ST). Changes in GP chain length, as number of carbon atoms in the sum of fatty acid moieties (*B*), GP saturation, as number of double bonds in the sum of fatty acid moieties (*C*), SP chain length, as number of carbon atoms in the sum of long chain base and fatty acid [values for odd numbered chain lengths ($n - 1$) were summed with values for the even numbered chain lengths (n) depicted] (*D*), SP saturation, as number of double bonds in the sum of long chain base and fatty acid (*E*), and SP hydroxylation (*F*) as calculated from individual quantities of lipid molecular species. (*G*) Changes in the content of SP species with three hydroxylations within each lipid class; they were not significant for SM but were highly significant for For, GM3, and Sulf (***). *P* values were estimated by one-way ANOVA ($n = 3$): $^*P < 0.05$; $^{**}P < 0.01$; $^{***}P < 0.001$. Error bars correspond to SD ($n = 3$).

Contact-Naive MDCK Cells and Polarization Assay. The MDCK cell culture is described in *SI Materials and Methods*. Cells are rendered contact-naive by replating them each day at a density of 11,000 cells/cm^2 for 3 d in medium with 10% (vol/vol) FCS [modified from the method of Yeaman (42)]. For polarization assays, these cells were seeded at the same density on polycarbonate filters and grown for 1, 3, 5, 7, 10, and 13 d. The medium was changed every second day.

EMT. MDCK B cells (from the laboratory of H.B.) expressing a retrovirally transduced DD-RafER fusion protein (20) were subcloned to generate clones that underwent epithelial polarization; uninfected MDCK B cells were also used in dense cell layers on porous supports. To induce EMT, cells were seeded <1/3 confluent on plastic and treated with 10^{-6} M estradiol for 2 d. Thereafter, the cells were trypsinized, seeded on porous supports as confluent monolayers, and treated with estradiol plus 5 mg/mL TGF-β for an additional 4 d. After that time, control cells formed fully polarized monolayers. Cells to be used for extraction were characterized as undergoing full EMT by morphology and markers.

ACKNOWLEDGMENTS. We thank those individuals working in the K.S. laboratory for both critical and positive feedback. We thank Christoph Thiele (Limes Center, University of Bonn, Bonn, Germany) for providing the synthetic internal standard phosphatidylinositol 17:0–17:0. We thank Ronny Herzog and Dominik Schwudke for helpful input in using the LipidXplorer software. We thank Roger Sandhoff for the quantification of GM3 and For standard extracts. K.S. was supported by the Deutsche Forschungsgemeinschaft "Schwerpunktprogramm1175" Grant SI459/2-1, Deutsche Forschungsgemeinschaft "Transregio 83" Grant TRR83 TP02, European Science Foundation "LIPIDPROD" Grant SI459/3-1, and Bundesministerium f. Bildung u. Forschung "ForMaT" Grant 03FO121. A.S. was supported by a virtual liver Grant Code/0315757 from the Bundesministerium f. Bildung u. Forschung.

1. Thiery JP, Acloque H, Huang RYJ, Nieto MA (2009) Epithelial-mesenchymal transitions in development and disease. *Cell* 139:871–890.
2. Nelson WJ (2009) Remodeling epithelial cell organization: Transitions between front-rear and apical-basal polarity. *Cold Spring Harb Perspect Biol* 1: a000513.
3. Leighton J, Estes LW, Mansukhani S, Brada Z (1970) A cell line derived from normal dog kidney (MDCK) exhibiting qualities of papillary adenocarcinoma and of renal tubular epithelium. *Cancer* 26:1022–1028.
4. Lever JE (1979) Regulation of dome formation in differentiated epithelial cell cultures. *J Supramol Struct* 12:259–272.
5. Bacallao R, et al. (1989) The subcellular organization of Madin-Darby canine kidney cells during the formation of a polarized epithelium. *J Cell Biol* 109:2817–2832.
6. Maschler S, et al. (2010) Annexin A1 attenuates EMT and metastatic potential in breast cancer. *EMBO Mol Med* 2:401–414.
7. Tanos B, Rodriguez-Boulan E (2008) The epithelial polarity program: Machineries involved and their hijacking by cancer. *Oncogene* 27:6939–6957.
8. van Meer G, Simons K (1986) The function of tight junctions in maintaining differences in lipid composition between the apical and the basolateral cell surface domains of MDCK cells. *EMBO J* 5:1455–1464.
9. Simons K, van Meer G (1988) Lipid sorting in epithelial cells. *Biochemistry* 27: 6197–6202.
10. Brasitus TA, Schachter D (1980) Lipid dynamics and lipid-protein interactions in rat enterocyte basolateral and microvillus membranes. *Biochemistry* 19:2763–2769.
11. Kawai K, Fujita M, Nakao M (1974) Lipid components of two different regions of an intestinal epithelial cell membrane of mouse. *Biochim Biophys Acta* 369:222–233.
12. Han X, Gross RW (2005) Shotgun lipidomics: Electrospray ionization mass spectrometric analysis and quantitation of cellular lipidomes directly from crude extracts of biological samples. *Mass Spectrom Rev* 24:367–412.
13. Ejsing CS, et al. (2009) Global analysis of the yeast lipidome by quantitative shotgun mass spectrometry. *Proc Natl Acad Sci USA* 106:2136–2141.
14. Dennis EA, et al. (2010) A mouse macrophage lipidome. *J Biol Chem* 285:39976–39985.
15. Liebisch G, et al. (2006) High throughput quantification of cholesterol and cholesteryl ester by electrospray ionization tandem mass spectrometry (ESI-MS/MS). *Biochim Biophys Acta* 1761:121–128.
16. Ejsing CS, et al. (2006) Automated identification and quantification of glycerophospholipid molecular species by multiple precursor ion scanning. *Anal Chem* 78: 6202–6214.
17. Schwudke D, et al. (2006) Lipid profiling by multiple precursor and neutral loss scanning driven by the data-dependent acquisition. *Anal Chem* 78:585–595.
18. Folch J, Lees M, Sloane Stanley GH (1957) A simple method for the isolation and purification of total lipides from animal tissues. *J Biol Chem* 226:497–509.
19. Hansson GC, Simons K, van Meer G (1986) Two strains of the Madin-Darby canine kidney (MDCK) cell line have distinct glycosphingolipid compositions. *EMBO J* 5: 483–489.
20. Lehmann K, et al. (2000) Raf induces TGFbeta production while blocking its apoptotic but not invasive responses: A mechanism leading to increased malignancy in epithelial cells. *Genes Dev* 14:2610–2622.
21. Lecat S, et al. (2000) Different properties of two isoforms of annexin XIII in MDCK cells. *J Cell Sci* 113:2607–2618.
22. Halbleib JM, Sääf AM, Brown PO, Nelson WJ (2007) Transcriptional modulation of genes encoding structural characteristics of differentiating enterocytes during development of a polarized epithelium in vitro. *Mol Biol Cell* 18:4261–4278.
23. Brügger B, et al. (2006) The HIV lipidome: A raft with an unusual composition. *Proc Natl Acad Sci USA* 103:2641–2646.
24. Chan R, et al. (2008) Retroviruses human immunodeficiency virus and murine leukemia virus are enriched in phosphoinositides. *J Virol* 82:11228–11238.
25. Takamori S, et al. (2006) Molecular anatomy of a trafficking organelle. *Cell* 127: 831–846.
26. Klenk HD, Choppin PW (1970) Glycosphingolipids of plasma membranes of cultured cells and an enveloped virus (SV5) grown in these cells. *Proc Natl Acad Sci USA* 66: 57–64.
27. Young WW, Jr., Lutz MS, Blackburn WA (1992) Endogenous glycosphingolipids move to the cell surface at a rate consistent with bulk flow estimates. *J Biol Chem* 267: 12011–12015.
28. Schwudke D, et al. (2007) Top-down lipidomic screens by multivariate analysis of high-resolution survey mass spectra. *Anal Chem* 79:4083–4093.
29. Hu Q, et al. (2005) The Orbitrap: A new mass spectrometer. *J Mass Spectrom* 40: 430–443.
30. Futerman AH, Riezman H (2005) The ins and outs of sphingolipid synthesis. *Trends Cell Biol* 15:312–318.
31. Breslow DK, Weissman JS (2010) Membranes in balance: Mechanisms of sphingolipid homeostasis. *Mol Cell* 40:267–279.
32. Meder D, Moreno MJ, Verkade P, Vaz WL, Simons K (2006) Phase coexistence and connectivity in the apical membrane of polarized epithelial cells. *Proc Natl Acad Sci USA* 103:329–334.
33. Karlsson K-A (1976) Aspects on structure and function of sphingolipids in cell surface membranes. *Structure of Biological Membranes*, ed Pascher SAal (Plenum, New York), p 245.
34. Carvalho M, et al. (2010) Survival strategies of a sterol auxotroph. *Development* 137: 3675–3685.
35. Ipsen JH, Karlström G, Mourtisen OG, Wennerström H, Zuckermann MJ (1987) Phase equilibria in the phosphatidylcholine-cholesterol system. *Biochimica Biophysica Acta* 905:162–172.
36. Niemelä PS, Hyvönen MT, Vattulainen I (2006) Influence of chain length and unsaturation on sphingomyelin bilayers. *Biophys J* 90:851–863.
37. Pike LJ, Han X, Chung KN, Gross RW (2002) Lipid rafts are enriched in arachidonic acid and plasmenylethanolamine and their composition is independent of caveolin-1 expression: a quantitative electrospray ionization/mass spectrometric analysis. *Biochemistry* 41:2075–2088.
38. Zech T, et al. (2009) Accumulation of raft lipids in T-cell plasma membrane domains engaged in TCR signalling. *EMBO J* 28:466–476.
39. Mishra R, Grzybek M, Niki T, Hirashima M, Simons K (2010) Galectin-9 trafficking regulates apical-basal polarity in Madin-Darby canine kidney epithelial cells. *Proc Natl Acad Sci USA* 107:17633–17638.
40. Guan F, Handa K, Hakomori SI (2009) Specific glycosphingolipids mediate epithelial-to-mesenchymal transition of human and mouse epithelial cell lines. *Proc Natl Acad Sci USA* 106:7461–7466.
41. Kumagai K, et al. (2005) CERT mediates intermembrane transfer of various molecular species of ceramides. *J Biol Chem* 280:6488–6495.
42. Yeaman C (2003) Ultracentrifugation-based approaches to study regulation of Sec6/8 (exocyst) complex function during development of epithelial cell polarity. *Methods* 30:198–206.